Bioactive Materials 6 (2021) 1140–1149

Contents lists available at ScienceDirect

Bioactive Materials

journal homepage: www.sciencedirect.com/journal/bioactive-materials

Nanomotor-based adsorbent for blood Lead(II) removal *in vitro* and in pig models

Meng Wang [a,1], Tianyi Bao [c,1], Wenqiang Yan [b], Dan Fang [a], Yueqi Yu [a], Zhiyong Liu [a], Guoyong Yin [c], Mimi Wan [a,**], Chun Mao [a,*], Dongquan Shi [b,***]

[a] National and Local Joint Engineering Research Center of Biomedical Functional Materials, School of Chemistry and Materials Science, Nanjing Normal University, Nanjing, 210023, PR China
[b] Department of Sports Medicine and Adult Reconstructive Surgery, Nanjing Drum Tower Hospital, The Affiliated Hospital of Nanjing University Medical School, Nanjing, 210008, PR China
[c] Department of Orthopaedics the First Affiliated Hospital of Nanjing Medical University, Nanjing, 210029, PR China

ARTICLE INFO

Keywords:
Heavy metal poisoning
Blood lead(II) poisoning
Magnetic nanomotor adsorbent
Alternating magnetic field
meso-2
3-Dimercaptosuccinic acid

ABSTRACT

Blood lead (Pb(II)) removal is very important but challenging. The main difficulty of blood Pb(II) removal currently lies in the fact that blood Pb(II) is mainly complexed with hemoglobin (Hb) inside the red blood cells (RBCs). Traditional blood Pb(II) removers are mostly passive particles that do not have the motion ability, thus the efficiency of the contact between the adsorbent and the Pb(II)-contaminated Hb is relatively low. Herein, a kind of magnetic nanomotor adsorbent with movement ability under alternating magnetic field based on Fe_3O_4 nanoparticle modified with meso-2, 3-dimercaptosuccinic acid (DMSA) was prepared and a blood Pb(II) removal strategy was further proposed. During the removal process, the nanomotor adsorbent can enter the RBCs, then the contact probability between the nanomotor adsorbent and the Pb(II)-contaminated Hb can be increased by the active movement of nanomotor. Through the strong coordination of functional groups in DMSA, the nanomotor adsorbent can adsorb Pb(II), and finally be separated from blood by permanent magnetic field. The *in vivo* extracorporeal blood circulation experiment verifies the ability of the adsorbent to remove blood Pb(II) in pig models, which may provide innovative ideas for blood heavy metal removal in the future.

1. Introduction

Lead (Pb) has been used by humans for thousands of years. However, it is not only a widespread environmental pollutant in the world, but also a toxic heavy metal with biohazard [1,2]. Natural Pb minerals are fully utilized in the chemical industry, printing and dyeing, smelting and other industrial activities, and then exist in the environment everywhere in the form of particles or ions [3,4]. From the late 19th and early 20th centuries, global Pb production began to rise rapidly. It was not until the 1970s that Pb was banned from use in gasoline additives [5]. Nonetheless, the impact on the health of humans, especially children caused by increasing Pb production and environmental pollution, remain a global problem [6]. So the US Agency for Toxic Substances and Disease Registry ranked Pb in second place on the priority list of dangerous substances [7].

Pb is nondegradable and accumulates in the body, which can have negative effects on the nervous, blood, kidney, cardiovascular and reproductive system in the body [8]. Especially for the nervous system, Pb still has irreversible nerve damage at lower exposure levels. For the blood system, Pb can inhibit the production of heme and cause anemia. Compared with adults, children have a higher absorption rate of Pb, and their intelligence and development are easily affected by adverse effects [9]. Pb exposure is estimated to account for 0.6% of the global burden of disease, among which developing regions are the most serious [10]. In developing countries, 143 million people die from Pb poisoning annually and more than 15 million children cause permanent nerve damage [11,12].

Pb can enter the body through the lungs breathing, skin contact, and

* Corresponding author.
** Corresponding author.
*** Corresponding author.
E-mail addresses: wanmimi@njnu.edu.cn (M. Wan), maochun@njnu.edu.cn (C. Mao), shidongquan1215@163.com (D. Shi).
[1] These authors contributed equally to this work.

https://doi.org/10.1016/j.bioactmat.2020.09.032
Received 24 July 2020; Received in revised form 17 September 2020; Accepted 29 September 2020
2452-199X/© 2020 The Authors. Production and hosting by Elsevier B.V. on behalf of KeAi Communications Co., Ltd. This is an open access article under the CC BY-NC-ND license (http://creativecommons.org/licenses/by-nc-nd/4.0/).

the gastrointestinal tract in daily diet. About 95% of Pb in the human body is deposited in bones and has a long half-life (20–30 years), while the other two parts of Pb are present in blood and other soft tissues with a half-life about 35–40 days. Bone Pb is an important source of blood Pb and soft tissue Pb, and there is a dynamic balance between the three parts. Under the current biomedical level, it is difficult to remove Pb from bones and soft tissues. Therefore, it is of great significance to study the removal of blood Pb [13–15]. Blood lead level (BLL) is considered the principal index human Pb content. The U. S. Center for Disease Control and Prevention (CDC) initially set the concentration of Pb(II) in children's blood at 10 μg dL^{-1}. Subsequently, it was modified to 5 μg dL^{-1} in 2012. However, children and adults will still be adversely affected even with minimal Pb exposure (BLL<5 μg dL^{-1}) [16,17]. The circulating Pb(II) in the blood is mainly located inside the red blood cells (RBCs) (>95%) and binds to hemoglobin (Hb), so it is very difficult to remove trace Pb(II) in blood [18].

The clinical treatments of Pb poisoning are hemodialysis and chelator therapy. During hemodialysis treatment, the patients need to receive dialysis for a long time and are likely to cause cardiovascular disease and other complications [19,20]. Chelating agents have been used in the detoxification of heavy metal Pb for more than 50 years, which is the current treatment method [21]. Traditional chelating agents are 2, 3-dimercaptopropanol (BAL) and ethylenediamine tetraacetate (EDTA). However, these early agents have been proved to be less effective and often have acute toxicity. The currently preferred chelating agent is hydrophilic meso-2, 3-dimercaptosuccinic acid (DMSA). Unlike BAL and EDTA, DMSA can be absorbed by the intestine nearly 50% after oral administration and will not redistribute toxic heavy metals from the surrounding organs to the brain to damage the nerves again [22,23]. However, this simple drug treatment mainly acts outside the cell and the treatment period is long (40–60 days), resulting in poor treatment effect [24].

When it comes to the research work, we summarized some of current Pb(II) removers in aqueous solutions, the current researches for the removal of heavy metals in the blood, and current researches of heavy metals by nanomotors to illustrate the novelty of the adsorbent used in this work. As shown in Table S1, at present, a large number of composite materials has been studied to remove the heavy metal Pb(II) in the wastewater environment, but there are few studies on the removal of Pb (II) in the blood due to the complex blood environment. Some of the Pb (II) removal materials in the aqueous solution are non-magnetic materials, which may be difficult to be separated when used in the blood. Meanwhile, the magnetic materials studied in the aqueous solution are difficult to be directly applied to the blood due to their larger size (most of them are micron scale) or poor biocompatibility [25–29]. Therefore, it is necessary to develop nanocomposites with good biocompatibility and easy separation for the study of blood Pb(II) adsorption *in vivo*. We further summarized the current research for the removal of heavy metals in blood. As shown in Table S2, several researchers have designed blood adsorbents with good biocompatibility in the blood. However, these removers mainly remove heavy metals in the plasma [30–32]. In view of these difficulties of blood heavy metal removal, we also proposed a strategy to remove blood Pb(II) located inside the RBCs [33]. However, this kind of adsorbent (passive nanoparticles) did not have the ability of autonomous movement in the RBCs, so it cannot fully contact with the Pb(II)-contaminated Hb, which may affect the actual removal efficiency.

Nanomotors can convert different types of energy to propel them in different fluids [34–36]. Therefore, the nanomotor technology was introduced into Pb(II) removal process. Existing research on the removal of heavy metals by nanomotors is mainly aimed at the aqueous solution (Table S3). Most of these nanomotors are driven by chemical toxic substances (such as hydrogen peroxide), which may have the limitation that it cannot be used in the internal environment [37,38]. It is reported that magnetic nanoparticles can be used as a magnetic nanomotor under the control of external magnetic field and have been proven to navigate within cells [39–41]. Therefore, the small-sized blood Pb(II) adsorbent designed in this work had good biocompatibility, and the alternating magnetic field was used as the driving force, and a reasonable blood Pb (II) removal mechanism was proposed, which is an improvement when compared with other materials (including materials or nanomotors used in aqueous condition or blood condition).

Specifically, a kind of magnetic nanomotor adsorbent based on small-sized Fe_3O_4 nanoparticle surface modified with meso-2, 3-dimercaptosuccinic acid (DMSA) was prepared and new blood Pb(II) removal strategy was further proposed. During the removal process, Fe_3O_4@DMSA can enter the RBCs, and the contact probability between the magnetic nanomotor adsorbent and the Pb(II)-contaminated Hb may be effectively increased by the active movement of magnetic nanomotor adsorbent. Then through the strong coordination of sulfydryl (or carboxyl), the magnetic nanomotor adsorbent can adsorb Pb(II), and finally was separated from the blood by permanent magnetic field (Fig. 1). The biocompatibility tests of magnetic nanomotor adsorbent, Pb(II) removal experiment *in vitro* and removal mechanism investigation, and the *in vivo* extracorporeal blood circulation experiment of living animal in pig models were carried out and discussed in detail.

2. Experimental section

2.1. Materials

Ferrous sulfate heptahydrate ($FeSO_4·7H_2O$), polyethylene glycol-20000 (PEG-20000), ammonia water ($NH_3·H_2O$), hydrogen peroxide (H_2O_2), toluene, dimethylsulfoxide (DMSO), 3-aminopropyltriethoxysilane (APTES) and lead acetate were obtained from Sinopharm Chemical Reagent Co., Ltd. (China). 5, 5′-dithiobis-2-nitrobenzoic acid (DTNB) and DMSA were purchased from Shanghai Macklin Reagent Co., Ltd. (China). APTT/PT/TT kits were brought from Shanghai Taiyang Biotech. Co., Ltd. (China). Peripheral blood lymphocyte extraction kit, CCK-8 and 3-(4, 5-dimethyl-2-thiazolyl)-2, 5-diphenyl-2-H-tetrazolium bromide (MTT) kits were purchased from Shanghai Solarbio Biotech. Co., Ltd. (China). TRITC phalloidin and Hoechst 33342 were obtained from Nanjing Anjieyou Biotech. Co., Ltd. (China).

2.2. Characterizations

The morphology and size of the samples were obtained by using TEM (Hitachi, H-7650, Japan). FT-IR was tested by using a Varian Cary 5000 FT-IR spectrophotometer. TGA was conducted using a TG analyzer (Netzsh, STA449F3, Germany) with process heating (from 25 to 850 °C, 10 °C min^{-1}) and N_2 flow (10 mL min^{-1}). Zeta potentials were tested by using Zetasizer Nano-Z instrument. The absorbance was measured on an ultraviolet–visible (UV–Vis) spectrophotometer (UV752, China). XRD was detected on Rigaku D/max 2500VL/PC. Hysteresis loop was detected by using vibrating sample magnetometer (VSM) of Lake Shore VSM-7404. The coagulation time was measured by a semi-automatic hemagglutination analyzer (Rayto, RT-2204C, China). The optical density (OD) value was obtained by using microplate reader (Bio-Rad, America). CLSM was observed the morphology of cells by Nikon Ti-E-A1R. XPS was tested by using Thermo Scientific ESCALAB250xi. Inductively coupled plasma (ICP) was used to measure the content of ions by IRIS Intrepid II.

2.3. The synthesis of Fe_3O_4

$FeSO_4·7H_2O$ (2.5 g) was dissolved in deionized water (30 mL) and transferred into a 100 mL round bottom flask. PEG-20000 (0.5 g) was dissolved in deionized water (10 mL). Then the solution was dropped into the flask and heated to 30 °C with mechanical stirring under N_2 atmosphere. $NH_3·H_2O$ (30 mL) was added and stirred vigorously for 10 min. Then H_2O_2 (0.27 mL) was added and stirred vigorously for 20 min. The reaction solution was transferred to a reaction kettle and reacted at 160 °C for 5 h. After the end, the solution was waited for cooling to room

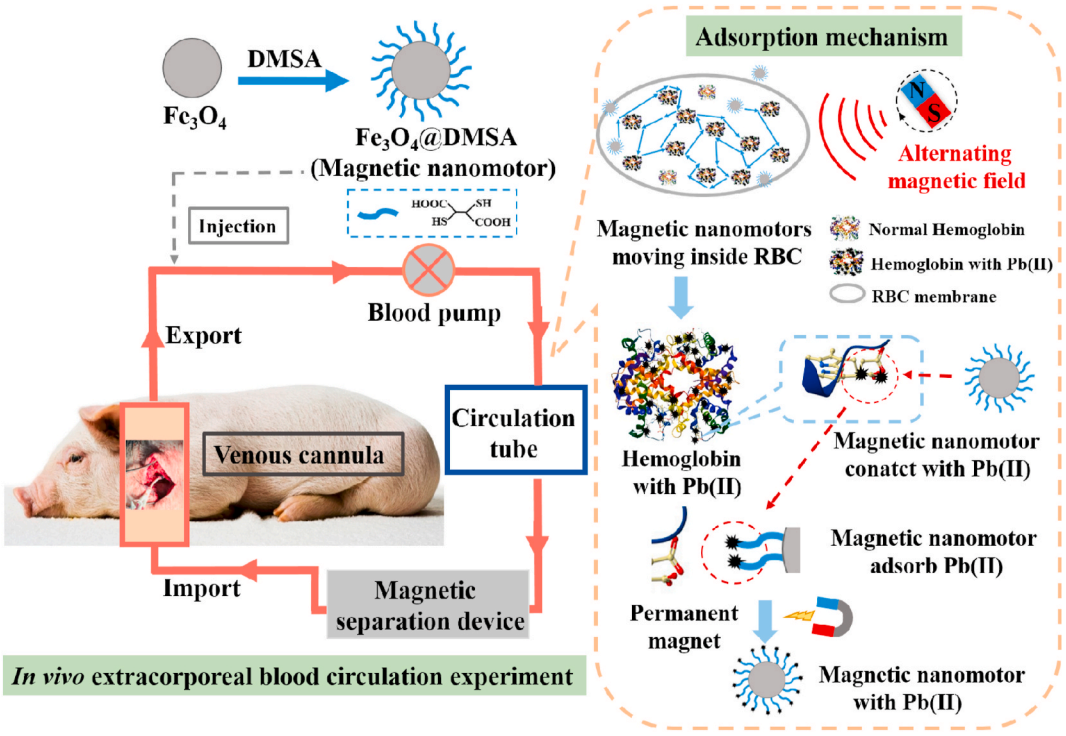

Fig. 1. Schematic diagram of the synthesis of magnetic nanomotor (Fe_3O_4@DMSA), *in vivo* extracorporeal blood circulation experiment and adsorption mechanism of the magnetic nanomotor.

temperature, and washed with water and ethanol for three times, respectively. The product was dried in an oven at 60 °C [42].

2.4. The synthesis of Fe_3O_4@DMSA

Fe_3O_4 (100 mg) was ultrasonically dispersed in toluene (10 mL) and the solution was added to a 50 mL round bottom flask, followed by mechanical stirring at room temperature. After N_2 was vented to expel air (15 min), DMSA (250 mg) was dissolved in DMSO (10 mL) and the solution was added dropwise to the flask. After N_2 was continuously introduced for 1 h, the reaction was closed until 12 h. The product was washing with water and ethanol for three times and dried in an oven at 60 °C to obtain Fe_3O_4@DMSA [43].

2.5. Determination of sulfhydryl content in Fe_3O_4@DMSA

The sulfhydryl content was determined by Ellman spectrophotometry [44]. DMSA was dissolved in anhydrous methanol solution (5 mmol L^{-1}). DTNB was dissolved in PBS solution (2 mg mL^{-1}). Different volumes of DMSA solution were taken into a 10 mL volumetric flask. Then DTNB solution (200 μL) and phosphate buffered solution (PBS) (8 mL) were added and then constant volume with deionized water. The solution was shaken and reacted for 5 min in the dark. The absorbance at 412 nm was measured by using a UV–Vis spectrophotometer. Fe_3O_4@DMSA (10 mg) was ultrasonically dispersed in anhydrous methanol solution (1 mL). Fe_3O_4@DMSA solution (200 μL) was added into a centrifuge tube, then DTNB solution (200 μL) and PBS solution (1 mL) were added and the solution was reacted at room temperature for 5 min. After the sample was magnetically separated, the supernatant was transferred to a 10 mL volumetric flask. The sample was magnetically washed with PBS solution (1 mL) for three times, and the washing solution was added to the volumetric flask. Then PBS solution (4 mL) was added to the volumetric flask and constant volume with deionized water. The absorbance at 412 nm was measured by using a UV–Vis spectrophotometer.

2.6. Biocompatibility test

The hemolysis rate was detected as follows. Firstly, fresh blood (4 mL) was centrifuged (2500 rpm, 10 min). The lower RBCs were obtained and added to PBS solution (5 mL) and the solution was centrifuged for twice (2500 rpm, 10 min). Then the RBCs were dispersed in PBS solution (100 mL) to make RBC suspension. Different amounts of Fe_3O_4@DMSA were added to the RBC suspension (3 mL) to prepare solutions (0.1, 0.2, 0.5, 1, 2 mg mL^{-1}). The solution was incubated at 37 °C for 30 min and then centrifuged (2500 rpm, 15 min). The OD value of upper liquid was read at 570 nm using a microplate reader. At the same time, deionized water was used as a positive control, and PBS solution was used as a negative control. Each experimental sample was tested three times in parallel. The hemolysis rate was calculated according to the OD value (Hemolysis rate=$(OD_{samples}-OD_{negative})/(OD_{positive}-OD_{negative}) \times 100\%$).

Similarly, Fe_3O_4 and Fe_3O_4@DMSA were added to the RBC suspension (3 mL, 2 mg mL^{-1}). After the solution was incubated at 37 °C for 30 min, the supernatant obtained by centrifugation was used to read the OD value at 570 nm using a microplate reader. Deionized water was used as a positive control, and PBS solution was used as a negative control. Each experimental sample was tested three times in parallel and the hemolysis rate was calculated. The solution before centrifugation was dropped on a glass slide, and the morphology of RBCs was observed with an optical microscope plus a digital camera.

The coagulation time was analyzed as follows. Fe_3O_4 and Fe_3O_4@DMSA (20 mg) were added to platelet-poor plasma (1 mL) and incubated at 37 °C for 30 min. Pure plasma was used as blank control group. APTT/PT/TT reagents were added in sequence according to the operation of the kits, and the coagulation time was tested by using a semi-automatic coagulation analyzer. Each sample was tested three times in parallel.

The CCK-8 cell viability test kit was used to evaluate the toxicity of Fe_3O_4@DMSA to peripheral blood lymphocytes. The peripheral blood lymphocyte suspension (10^5-10^6 cells/well) was added to 96-well plate, and the Fe_3O_4@DMSA-medium solution (10 μL/well) was added to form solutions with different concentrations (0.1, 1, 2.5, 5 mg mL^{-1}). At the

same time, blank group without cells and blank group with cells were set as controls. After 96-well plate was incubated at 37 °C for 1 h, CCK-8 solution (10 μL) was added and incubated for 4 h. The OD value was obtained at 450 nm by using microplate reader. Each sample was tested three times in parallel. The cell activity was calculated as: Cell viability= (OD_{sample}-$OD_{without\ cell}$)/($OD_{with\ cell}$-$OD_{without\ cell}$) × 100%.

2.7. Interaction between Fe_3O_4@DMSA and RBCs

Fe_3O_4@DMSA (10 mg) was added to fresh blood (2 mL) and incubated at 37 °C for 30 min. Glutaraldehyde solution (2 mL, 2.5%) was added and mixed for 1 h to fix RBCs morphology. After the solution was centrifuged (2500 rpm, 10 min), RBCs were obtained. In order to remove excess water, ethanol solution (50%, 60%, 70%, 80%, 90%) was added to the RBCs, and then the solution was centrifuged (2500 rpm, 10 min). Finally, the RBCs were dispersed in absolute ethanol and observed by using TEM.

Fe_3O_4@DMSA (30 mg) was dispersed in ethanol solution (30 mL, 50%). APTES (100 μL) and FITC reagent (200 μL) was added and reacted at 40 °C for 24 h in the dark to load Fe_3O_4@DMSA with fluorescence. Fe_3O_4@DMSA-FITC was incubated with the RBC suspension for 30 min (5 mg mL^{-1}). The glutaraldehyde solution (100 μL, 2.5%) was added and the PBS solution was added to rinse twice. The dye of TRITC phalloidin was added to stain the RBCs for 20 min, and then the solution was rinsed three times with PBS, and observed under CLSM.

2.8. Pb(II) adsorption test in vitro of magnetic nanomotor adsorbent

Fresh Pb(II) poisoned blood (1 mL, 0.1 ppm) was added with Fe_3O_4@DMSA (5 mg) and placed under static and alternating magnetic field for 0.5 h. After the sample was sufficiently separated with a permanent magnetic field, the upper blood (0.5 mL) was taken into a Teflon reactor. H_2O_2 (1.5 mL) and HNO_3 (1 mL) were added, and the reaction was carried out at 180 °C for 2 h under high temperature and high pressure to digest the blood. After the reaction, the liquid was transferred to a 5 mL volumetric flask and made up to volume with purified water. ICP was used to measure the concentration of Pb(II) in blood before and after adsorption [45,46]. The adsorption efficiency was calculated as: E=(C_0–C_1)/C_0 × 100%, where C_0 was the concentration of before adsorption, and C_1 was the concentration of after adsorption.

2.9 In vivo extracorporeal blood circulation experiment of living animal

The anesthetic surgical and postoperative care protocols of animal experiments were examined and approved by the Animal Ethics Committee of Nanjing Drum Tower Hospital and conducted under the Institutional Committee of Care and Use of Laboratory Animals. The Bama miniature pigs was used as experimental pigs (female, 50 kg, n = 3). Animal models of Pb(II) poisoning were established by feeding lead acetate (1.5 g day^{-1}, 10 day) [47]. Pig of the control group was detoxified by oral DMSA (0.5 g day^{-1}, 7 day) [48]. The *in vivo* extracorporeal blood circulation experiment was established as follows: The experimental pig was anesthetized and the upper layer of tissue was cut in the neck. Blood was drawn after cannulation at the vein. Fe_3O_4@DMSA (3 g) was injected and mixed with blood, passed through an external circulation tube, and separated by a permanent magnetic field. The separated blood was led back to the porcine artery [49]. The blood flow rate was 20 mL min^{-1}. The adsorbent concentration was 5 mg mL^{-1}. After the second circulation, the main organ tissues of the pig were cut and stained, then observed and photographed under an optical microscope [50]. The blood before and after the two circulations was digested at high temperature (180 °C, 2 h). ICP was used to test Pb(II) concentration and the elemental Fe content in the blood before and after the two circulations, then the adsorption efficiency and the material residual rate were calculated.

3. Results and discussion

3.1. Characterization of Fe_3O_4@DMSA

The morphology and size of Fe_3O_4@DMSA were observed by using transmission electron microscopy (TEM). As shown in Fig. 2A and B, the synthesized Fe_3O_4 nanoparticles are uniformly dispersed, with a mean size of approximately 35 nm. After DMSA modification, there was no obvious change in morphology and size. The scanning electron microscope-mapping (SEM-mapping) and energy-dispersive spectroscopy (EDS) of Fe_3O_4@DMSA are shown in Fig. S1, where the C and S elements can be attributed to related elements in DMSA. The successful preparation of Fe_3O_4@DMSA can be further confirmed by the Fourier transform infrared spectroscopy (FT-IR) spectrum and zeta potential measurements. The peak at around 576 cm^{-1} in the FT-IR spectrum can be attributed to the lattice vibration of Fe–O in Fe_3O_4 [51,52]. The peaks at 1630 cm^{-1} and 1379 cm^{-1} are related to –COO– asymmetric and symmetric stretching vibration (Fig. 2C). After DMSA was used for modification, it is difficult to observe the characteristic peaks of sulfhydryl groups by FT-IR spectroscopy [53–57]. Ellman spectrophotometry was used to detect the sulfhydryl content in Fe_3O_4@DMSA [58,59]. The sulfhydryl group in Fe_3O_4@DMSA was calculated from the standard curve of Fig. 2D to be approximately 0.049 mmol g^{-1}. Pure Fe_3O_4 exhibited a weak negative charge (−4.3 mV), and the zeta potential of Fe_3O_4@DMSA became −18.1 mV (Fig. 2E), which may be due to the modification of the negatively charged DMSA [60]. The modification amount of DMSA can be determined by thermogravimetric analysis (TGA) [61]. As shown in Fig. 2F, the ratio of DMSA in Fe_3O_4@DMSA was about 7.8%. X-ray diffraction (XRD) results showed that Fe_3O_4@DMSA still retained the crystal planes at (220), (311), (400), (422), (511) and (440) of Fe_3O_4, indicating that the original cubic inverse spinel structures was not destroyed by the modification process (Fig. 2G) [62,63]. The hysteresis loops showed that the modification did not affect the magnetic properties of the Fe_3O_4, ensuring that the sample can be effectively separated and recovered, and the low hysteresis indicated that Fe_3O_4@DMSA can be better controlled by the alternating magnetic field (Fig. 2H) [64,65].

3.2. Biocompatibility of Fe_3O_4@DMSA

The determination of hemolysis rate is very important for blood compatibility. International standards of hemolysis rate for non-hemolytic biomaterials is below 2%, whereas >5% is hemolytic materials [66,67]. When Fe_3O_4 was modified with DMSA, the hemolysis rate decreased from 2.7% to 1.9%, indicating that DMSA can improve the blood compatibility of the material (Fig. S2A). The hemolysis rates of Fe_3O_4@DMSA at different concentrations were shown in Fig. 3A. The hemolysis rate was still below 2% at the higher concentration of Fe_3O_4@DMSA. The RBC morphology results showed that after incubation of Fe_3O_4@DMSA with RBCs, the RBCs still had the normal morphology (Fig. S2B), illustrating that Fe_3O_4@DMSA would not cause significant damage to RBCs [68]. Activated partial thromboplastin time/prothrombin time/thrombin time (APTT/PT/TT) results proved that Fe_3O_4@DMSA had no significant effect on the coagulation system compared with blank plasma (Fig. 3B). Cell counting kit-8 (CCK-8) was used to evaluate the cytotoxicity of Fe_3O_4@DMSA on peripheral blood lymphocytes. When different concentrations of Fe_3O_4@DMSA were incubated with peripheral blood lymphocytes for 1 h, the cell viability remained above 90%, indicating that Fe_3O_4@DMSA has good cell compatibility (Fig. 3C).

3.3. Study on the interaction between Fe_3O_4@DMSA and cells

More than 95% of blood Pb(II) will bind to RBCs (especially the Hb), and less than 5% of blood Pb(II) is present in plasma. Therefore, how to remove Pb(II) bound to Hb in RBCs is the key to treating blood Pb(II)

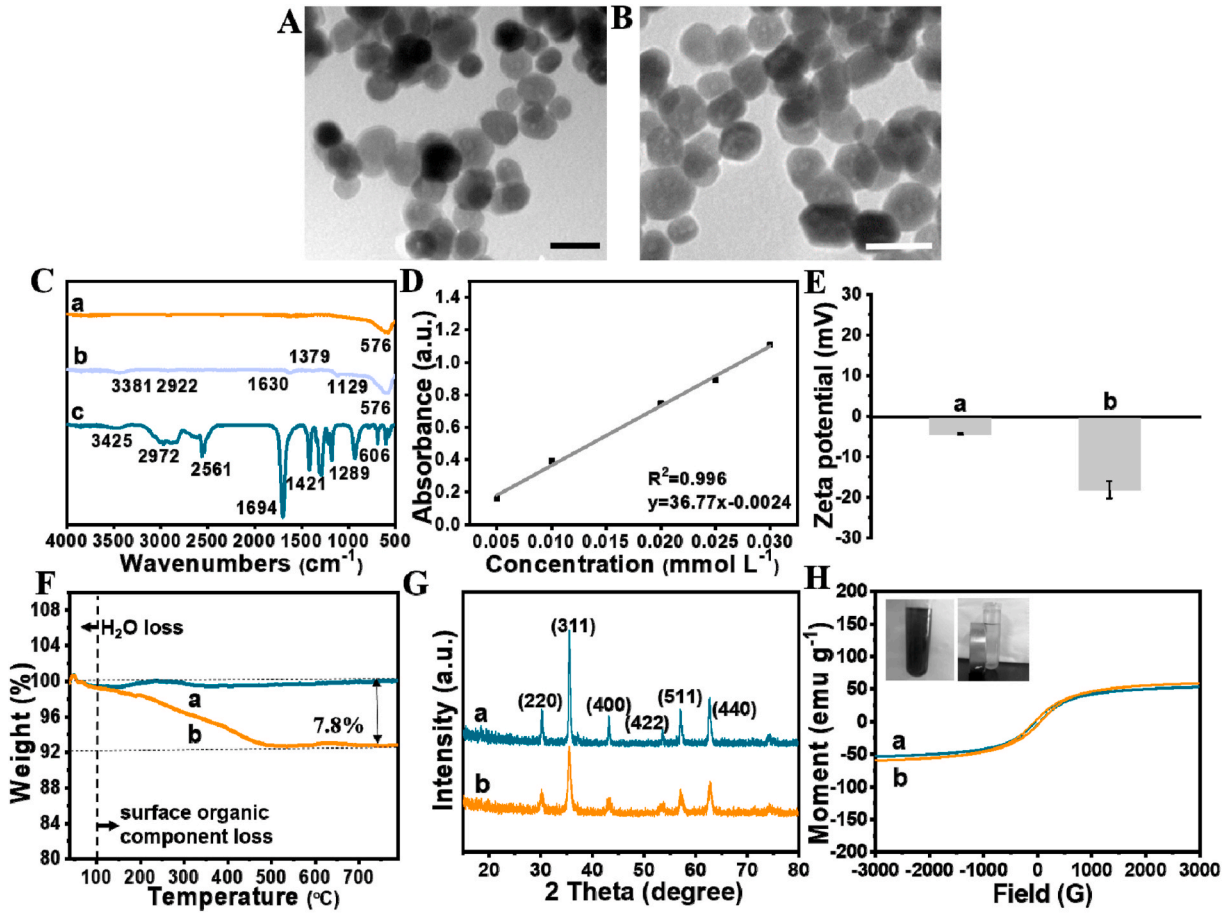

Fig. 2. TEM images of (A) Fe_3O_4, (B) Fe_3O_4@DMSA (scale bar: 50 nm); (C) FT-IR spectra of (a) Fe_3O_4, (b) Fe_3O_4@DMSA, (c) DMSA; (D) Standard curve of quantitative sulfhydryl groups in DMSA; (E) Zeta potentials of (a) Fe_3O_4, (b) Fe_3O_4@DMSA; (F) TGA measurements of (a) Fe_3O_4, (b) Fe_3O_4@DMSA; (G) XRD of (a) Fe_3O_4, (b) Fe_3O_4@DMSA; (H) Hysteresis loops of (a) Fe_3O_4, (b) Fe_3O_4@DMSA (inset: the sample was separated by a magnet).

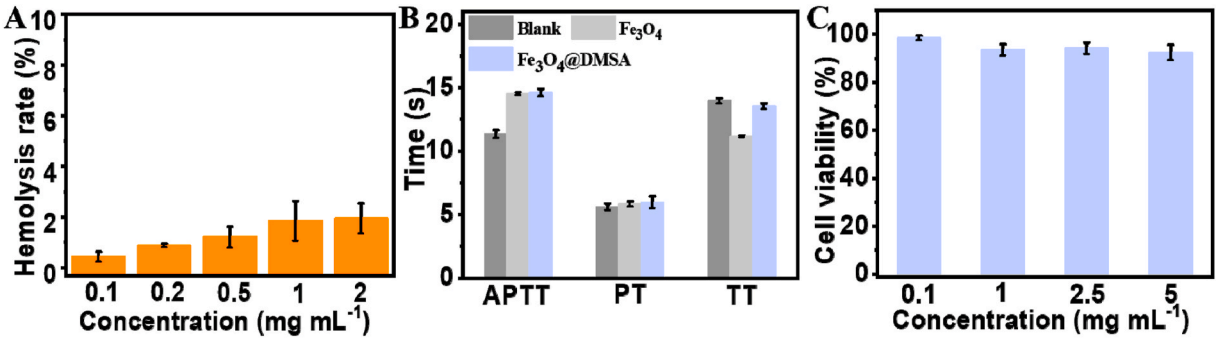

Fig. 3. (A) Hemolysis rate at different concentrations of Fe_3O_4@DMSA; (B) APTT, PT and TT for different samples; (C) CCK-8 at different concentrations of Fe_3O_4@DMSA.

poisoning. It has been regarded that nanoparticles larger than 1 μm may be left on the outside of RBCs, but smaller size can enter RBCs and be separated by permanent magnetic field [69–71]. TEM was used to observe the interaction between the Fe_3O_4@DMSA and RBCs. Compared with blank RBCs, a large number of nanoparticles entered the RBCs after Fe_3O_4@DMSA was incubated with the RBCs (Fig. 4A). Fe_3O_4@DMSA was loaded with the green fluorescent dye fluoresceine isothiocyanate (FITC) and incubated with RBCs whose cytoskeleton was stained red by tetramethyl rhodamine isothiocynate (TRITC) phalloidin. Confocal laser scanning microscopy (CLSM) images (Fig. 4B) and three-dimensional (3D) tomography (Movie S1) showed that Fe_3O_4@DMSA entered the RBCs instead of attaching to the RBC surface. Furthermore, the interaction between Fe_3O_4@DMSA and macrophage RAW264.7 was shown in Figs. S3, S4 and Tables S4 and S5, indicating that Fe_3O_4@DMSA can effectively avoid the phagocytosis of the immune system (see the supporting information for detailed analysis).

Supplementary data related to this article can be found at https://doi.org/10.1016/j.bioactmat.2020.09.032.

3.4. Study on adsorption efficiency and adsorption mechanism of Pb(II) by magnetic nanomotor adsorbent in vitro

The magnetic nanomotor has been proven to be manipulated within the cell. Therefore, when the magnetic nanomotor adsorbent was

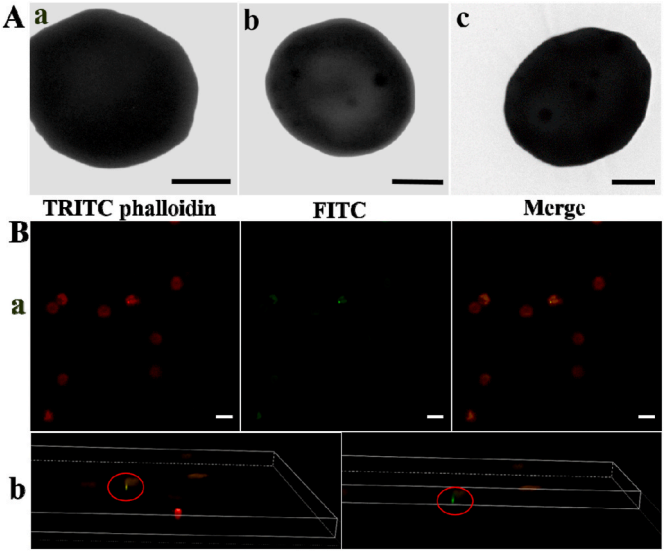

Fig. 4. (A) TEM images of (a) blank RBC, (b, c) RBC contacting with Fe_3O_4@DMSA (scale bar: 2 μm); (B) CLSM images of (a) RBC (stained with red dye TRITC phalloidin) uptake of the Fe_3O_4@DMSA (labeled with green dye FITC) (scale bar: 10 μm), (b) screenshot of 3D rendered Movie S1.

incubated with the RBCs and entered the RBCs, Fe_3O_4@DMSA nanoparticles can be controlled to move inside the RBCs through the alternating magnetic field, and the adsorption performance of the magnetic nanomotor adsorbent was also explored. First, the magnetic nanomotor adsorbent can quickly move inside the RBCs under the action of an alternating magnetic field, indicating that this autonomous movement may effectively increase the contact probability of the magnetic nanomotor adsorbent and the Pb(II)-containing Hb inside the RBCs (Fig. 5A and Movie S2). The adsorption efficiencies in the Pb(II)-poisoned blood *in vitro* are shown in Fig. S5. The optimal adsorption condition of Fe_3O_4@DMSA in blood (0.1 ppm) was set as 5 mg mL^{-1} for 0.5 h (see the supporting information for detailed analysis). As shown in Fig. 5B, after Fe_3O_4@DMSA (5 mg mL^{-1}) was incubated with Pb(II)-poisoned blood (0.1 ppm) for 0.5 h, the adsorption efficiency of the magnetic nanomotor adsorbent under static condition was only 40.6%. However, the magnetic nanomotor adsorbent under the condition of continuous alternating magnetic field had an adsorption efficiency of 80.6%, which doubled compared with that at the static condition, indicating that the active movement of the magnetic nanomotor adsorbent may effectively increase the contact probability of the magnetic nanomotor adsorbent and the Pb(II)-containing Hb in the RBCs, thus the adsorption efficiency was also greatly improved. Meanwhile, ion selectivity is also a key factor in the effective adsorption of adsorbents in blood [72,73]. Fig. S6 showed that the magnetic nanomotor adsorbent had high adsorption efficiency (reached 80%) for heavy metal Pb(II), and did not obvious effect on other normal ions, indicating that the magnetic nanomotor adsorbent had a good selectivity for Pb(II) in blood.

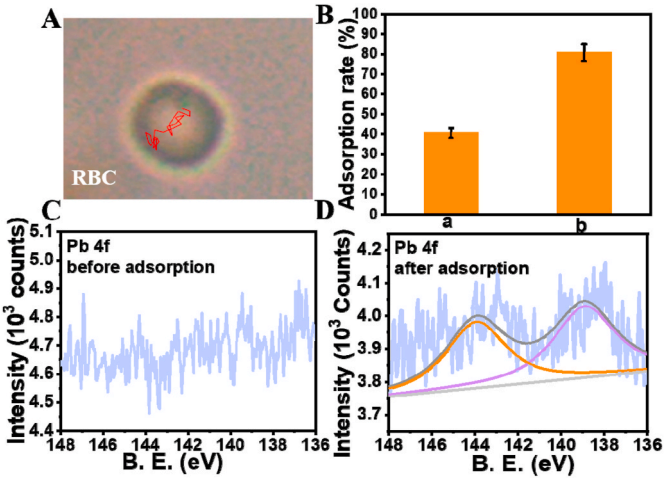

Fig. 5. (A) The trajectory of magnetic nanomotor adsorbent in RBC from Movie S2 (time: 10 s); (B) Adsorption rates of Fe_3O_4@DMSA (5 mg mL^{-1}) in blood (0.1 ppm) at (a) static, (b) shaking at the alternating magnetic field for 0.5 h; XPS spectra (Pb 4f) of Fe_3O_4@DMSA (C) before and (D) after adsorption in blood.

Supplementary data related to this article can be found at https://doi.org/10.1016/j.bioactmat.2020.09.032.

In order to study the adsorption mechanism of the magnetic nanomotor adsorbent, the adsorption capacity of the magnetic nanomotor adsorbent in aqueous solution was explored (Fig. S7). As shown in Fig. S7A, the adsorption reached equilibrium when the adsorbent concentration was 5 mg mL^{-1} (consistent with that in blood condition). Adsorption isotherm and adsorption kinetics models are commonly applied for describing the adsorption behavior of the metal ion [74–76]. Compared with Langmuir equation ($R^2 = 0.981$), the removal process was more consistent with Freundlich equation ($R^2 = 0.994$, $n = 0.887 < 1$) (Figs. S7B, S8 and Table S6). This indicated the chemisorption process of Pb(II) on heterogeneous multilayer surface of the magnetic nanomotor adsorbent. At the same time, compared with the pseudo-first-order kinetics, the adsorption process is more in line with the pseudo-second-order kinetics (Fig. S7C, S9 and Table S7) [77,78]. X-ray photoelectron spectroscopy (XPS) was used to analyze the changes of surface elemental states before and after magnetic nanomotor adsorbent adsorbed Pb(II) in the blood. After Fe_3O_4@DMSA was separated from the blood with permanent magnetic field, the peaks of Pb 4f were appeared at around 138.9 eV and 143.9 eV, proving that Fe_3O_4@DMSA effectively adsorbed and brought out Pb(II) from the blood (Fig. 5C and D) [79,80]. The O 1s spectrum at around 529.6 eV and 531.5 eV were corresponded to O–C═O and C=O of the carboxyl functional group, respectively. And the new peak at around 530.2 eV after adsorption can be attributed to the formation of Pb–O [56,81,82]. In the S 2p spectrum, the peak at around 163.3 eV was the free sulfhydryl functional group, and the peak at around 164.0 eV was the disulfide bond after oxidation in the synthesis process [83,84]. After adsorption, the sulfhydryl group of Fe_3O_4@DMSA changed and the peak corresponding to the disulfide bond did not change significantly, indicating that the sulfhydryl groups also acted on the adsorption of blood Pb(II) (Fig. S10).

Since most of the Pb(II) in RBCs are bound to Hb, in order to verify whether the binding strength of the magnetic nanomotor adsorbent with Pb(II) was greater than the binding strength of Hb and Pb(II), theoretical calculation method was used to study. As shown in Fig. S11, the binding energies of Pb(II) and amino acid fragments of Asp380, Asp384, and Asp386 in Hb were about 53.40, 95.50, and 79.30 kcal mol^{-1} (Table S8), which were less than the binding energy of sulfhydryl group and Pb(II) (107.58 kcal mol^{-1}). This theoretically confirmed the possibility that magnetic nanomotor adsorbent with sulfhydryl groups can adsorb Pb(II) in Hb.

Therefore, the adsorption mechanism of the magnetic nanomotor adsorbent in blood was speculated as follows. When Fe_3O_4@DMSA entered the blood environment, the magnetic nanomotor adsorbent can enter the inside of the RBCs and the contact probability between Fe_3O_4@DMSA and the Pb(II)-containing Hb may be effectively increased based on the active movement of magnetic nanomotor adsorbent under the condition of continuous alternating magnetic field. Through coordination interaction, the sulfhydryl groups (or small amount of carboxyl functional groups) in the Fe_3O_4@DMSA adsorbed the Pb(II) in Hb. Finally, the Fe_3O_4@DMSA with Pb(II) was safely removed by permanent magnetic field.

3.5. *In vivo* extracorporeal blood circulation experiment of living animal

Finally, the adsorbent was applied to animal model of Pb(II) poisoning. Due to the lack of existing magnetic manipulation technology and devices, it is difficult for the magnetic nanomotor adsorbent under the action of the alternating magnetic field to pass precise control force to ensure that it can safely and effectively act on most of the RBCs in the macroscopic blood for a long time [39]. In addition, the existing animal blood Pb(II) removal scheme requires fast blood circulation, which has a great influence on the autonomy of the magnetic nanomotor, making the current magnetic motor adsorbent extremely difficult to apply to the study of blood Pb(II) adsorption in large animal models. Therefore, extracorporeal blood circulation device was constructed to investigate the adsorption efficiency of blood Pb(II) adsorbent Fe_3O_4@DMSA under non-magnetic field control. The specific operation and device structure were shown in Fig. 6A. As shown in Fig. 6B, the seven-day treatment efficiency of the control group was about 39%. In the *in vivo* extracorporeal blood circulation experiments, the efficiency of the first circulation was about 43% and the second adsorption efficiency was about 51% after 50 min of treatment with the adsorbent. After the two circulations, the Pb(II) concentration in pig blood was dropped to lower lever (0.098 ppm). The above results indicated that the adsorbent can be used to reduce blood Pb(II) levels in animal model efficiently. At the same time, the routine blood tests showed that two circulations did not affect the contents of RBCs and Hb in the blood (Fig. 6C and D). As shown in Fig. S12, there was no significant change in the levels of various enzymes in the blood after the surgery. The normal ion content and the content of gas (CO_2 and NO) did not change significantly after the two circulations (Figs. S13 and S14). Compared with the organ tissue section of the control group (DMSA), there was no inflammation in the organs after the surgery (Fig. 6E). When the blood circulation experiment was carried out, the adsorbent was mainly used to act in the extracorporeal circulation tube and separated before the blood was returned to the pig. Considering the possibility of the adsorbent entered the body, the content of elemental Fe in the blood before and after the two circulations was also detected. After the second circulation, the increased Fe content in the blood was less than 1%, indicating that the adsorbent can be effectively separated from the blood.

4. Conclusion

In summary, a magnetic nanomotor adsorbent for blood Pb(II) removal based on small-sized Fe_3O_4 nanoparticle surface modified with the chelating agent DMSA was proposed, which can move in the RBCs under alternating magnetic field. The nanomotor concept were introduced in blood Pb(II) adsorption process, which has never been reported before. This magnetic nanomotor adsorbent can enter the inside of RBCs and the contact probability between the nanomotor adsorbent and the Pb(II)-containing Hb can be effectively increased based on the active movement of the nanomotor. Then Pb(II) bound to Hb can be adsorbed by the magnetic nanomotor adsorbent through the strong coordination of sulfydryl (or carboxyl). The biocompatibility tests show that the

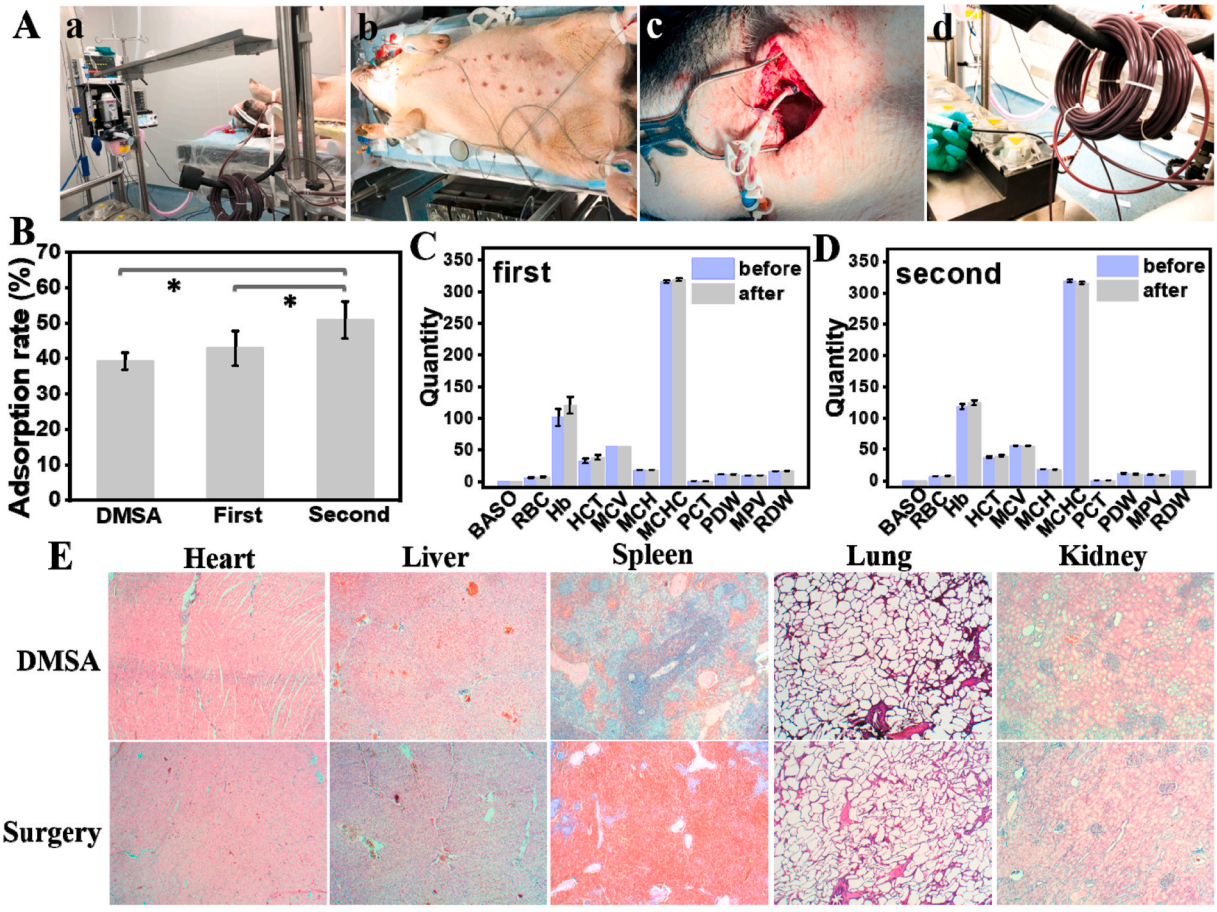

Fig. 6. (A) Animal experiment with *in vivo* surgery of (a) experimental monolithic apparatus, (b) pig undergoing surgery, (c) venous cannula, (d) nanomotor injection and extracorporeal blood circuit; (B) Removal efficiency of Pb(II) in blood of pigs by oral treatment (DMSA, 7 days), and Fe_3O_4@DMSA treatment after the first and the second circulation (20 mL min^{-1}); (C, D) Routine blood test for the first and second circulation; (E) Tissue histology of the main organs of pigs in oral DMSA group and surgery group (magnification: 40 ×). *Denotes statistical significance between bars (*for $p < 0.05$) using one-way ANOVA analysis. Experimental data are mean ± s.d. of samples in a representative experiment (n = 3).

adsorbent does not cause obvious hemolysis and coagulation of the blood. Compared with previous studies on blood Pb(II) adsorption, the magnetic nanomotor adsorbent shows better selective adsorption efficiency in Pb(II) poisoning blood *in vitro*. An extracorporeal blood circulation device was constructed to remove Pb(II) in pig models, further proving the adsorbent has good removal performance (first circulation: 43%/50 min, second circulation: 51%/50 min). These results verify that the combination of surface interface modification technology and nanomotor technology may provide important technical support for the removal of blood Pb(II).

CRediT authorship contribution statement

Meng Wang: Writing - original draft, Methodology, Software, Formal analysis. **Tianyi Bao:** Investigation, Software, Formal analysis. **Wenqiang Yan:** Methodology, Formal analysis. **Dan Fang:** Investigation, Formal analysis. **Yueqi Yu:** Software, Data curation. **Zhiyong Liu:** Data curation. **Guoyong Yin:** Methodology. **Mimi Wan:** Writing - review & editing, Conceptualization, Funding acquisition. **Chun Mao:** Supervision, Writing - review & editing, Funding acquisition. **Dongquan Shi:** Resources, Funding acquisition.

Declaration of competing interest

Authors claim no conflicts of interest.

Acknowledgements

The work was supported by Social development project of Jiangsu Natural Science Foundation (No: BE2019744), Jiangsu Collaborative Innovation Center of Biomedical Functional Materials, National Natural Science Foundation of China (51641104, 21603105), Natural Science Foundation of Jiangsu Province (BK20171115), and the Priority Academic Program Development of Jiangsu Higher Education Institution.

Appendix B. Supplementary data

Supplementary data to this article can be found online at https://doi.org/10.1016/j.bioactmat.2020.09.032.

References

[1] G. Corsetti, C. Romano, A. Stacchiotti, E. Pasini, F.S. Dioguardi, Endoplasmic reticulum stress and apoptosis triggered by sub-chronic lead exposure in mice spleen: a histopathological study, Biol. Trace Elem. Res. 178 (2017) 86–97, https://doi.org/10.1007/s12011-016-0912-z.

[2] C.B. Kim, S. Shin, S.-H. Song, Hemorheological changes caused by lead exposure, Clin. Hemorheol. Microcirc. 55 (2013) 341–348, https://doi.org/10.3233/CH-2012-1641.

[3] T.M.A. Shaikh, Adsorption of Pb(II) from wastewater by natural and synthetic adsorbents, Biointerface Res. Appl. Chem. 10 (2020) 6522–6539, https://doi.org/10.33263/BRIAC105.65226539.

[4] M.R. Awual, An efficient composite material for selective lead(II) monitoring and removal from wastewater, J. Environ. Chem. Eng. 7 (2019) 103087, https://doi.org/10.1016/j.jece.2019.103087.

[5] P.J. Landrigan, Lead and the heart: an ancient metal's contribution to modern disease, Lancet Public Health 3 (2018) e156, https://doi.org/10.1016/S2468-2667(18)30043-4.

[6] M. Ahamed, S. Singh, J.R. Behari, A. Kumar, M.K.J. Siddiqui, Interaction of lead with some essential trace metals in the Blood of Anemic Children from Lucknow, India, Clin. Chim. Acta 377 (2007) 92–97, https://doi.org/10.1016/j.cca.2006.08.032.

[7] ATSDR, ATSDR Substance Priority List, 2018 accessed, https://www.atsdr.cdc.gov/spl/. (Accessed September 2018).

[8] S.H. Li, Y. Yao, T. Zhao, M.L. Wang, F. Wu, Biochars preparation from waste sludge and composts under different carbonization conditions and their Pb(II) adsorption behaviors, Water Sci. Technol. 80 (2019) 1063–1075, https://doi.org/10.2166/wst.2019.353.

[9] K. Neeti, T. Prakash, Effects of heavy metal poisoning during pregnancy, Int. Res. J. Environ. Sci. 2 (2013) 88–92.

[10] World Health Organization, Ten Chemicals of Major Public Health Concern, 2008 accessed, https://www.who.int/ipcs/assessment/public_health/chemicals_phc/en/. (Accessed September 2018).

[11] M.R. Awual, M.M. Hasan, A. Islam, M.M. Rahman, A.M. Asiri, M.A. Khaleque, M. C. Sheikh, Offering an innovative composited material for effective lead(II) monitoring and removal from polluted water, J. Clean. Prod. 231 (2019) 214–223, https://doi.org/10.1016/j.jclepro.2019.05.125.

[12] V. Keshav, P. Franklyn, K. Kondiah, Recombinant fusion protein PbrD cross-linked to calcium alginate nanoparticles for Pb remediation, ACS Omega 4 (2019) 16816–16825, https://doi.org/10.1021/acsomega.9b01624.

[13] N.C. Papanikolaou, E.G. Hatzidaki, S. Belivanis, G.N. Tzanakakis, A.M. Tsatsakis, Lead toxicity update. a brief review, Med. Sci. Mon. Int. Med. J. Exp. Clin. Res. 11 (2005) RA329–336, https://doi.org/10.1051/medsci/20052110888.

[14] H.-Y. Chuang, J. Schwartz, T. Gonzales-Cossio, M.C. Lugo, E. Palazuelos, A. Aro, H. Hu, M. Hernandez-Avila, Interrelations of lead levels in bone, venous blood, and umbilical cord blood with exogenous lead exposure through maternal plasma lead in peripartum women, Environ. Health Perspect. 109 (2001) 527, https://doi.org/10.2307/3454713, 523.

[15] M.B. Rabinowitz, Toxicokinetics of bone lead, Environ. Health Perspect. 91 (1991) 33–37, https://doi.org/10.2307/3430979.

[16] Y.R. Chen, X.J. Xu, Z.J. Zeng, X.Q. Lin, Q.L. Qin, X. Huo, Blood lead and cadmium levels associated with hematological and hepatic functions in patients from an e-waste-polluted area, Chemosphere 220 (2019) 531–538, https://doi.org/10.1016/j.chemosphere.2018.12.129.

[17] Y.Y. Wu, J.N. Lou, X. Sun, L.N.Q. Ma, J.Y. Wang, M.Y. Li, H. Sun, H.B. Li, L. Huang, Linking elevated blood lead level in urban school-aged children with bioaccessible lead in neighborhood soil, Environ. Pollut. 261 (2020) 114093, https://doi.org/10.1016/j.envpol.2020.114093.

[18] T. Sakai, Biomarkers of lead exposure, Ind. Health 38 (2000) 127–142, https://doi.org/10.2486/indhealth.38.127.

[19] J.-L. Lin, D.-T. Lin-Tan, C.-W. Hsu, T.-H. Yen, K.-H. Chen, H.-H. Hsu, T.-C. Ho, K.-H. Hsu, Association of blood lead levels with mortality in patients on maintenance hemodialysis, Am. J. Med. 124 (2011) 350–358, https://doi.org/10.1016/j.amjmed.2010.10.022.

[20] L. Paolo, Z. Luca, G. Antonio, S.S. Salvatore, C. Pietro, D.A. Roberto, Kidney and heavy metals-the role of environmental exposure (review), Mol. Med. Rep. 15 (2017) 3413–3419, https://doi.org/10.3892/mmr.2017.6389.

[21] A. Mehta, S.J.S. Flora, Possible role of metal redistribution, hepatotoxicity and oxidative stress in chelating agents induced hepatic and renal metallothionein in rats, Food Chem. Toxicol. 39 (2001) 1029–1038, https://doi.org/10.1016/S0278-6915(01)00046-1.

[22] J. Aasetha, M.A. Skaug, Y. Cao, O. Andersen, Chelation in metal intoxication-Principles and paradigms, J. Trace Elem. Med. Biol. 31 (2015) 260–266, https://doi.org/10.1016/j.jtemb.2014.10.001.

[23] F.A. Soares, M. Farina, F.W. Santos, D. Souza, J.B.T. Rocha, C.W. Nogueira, Interaction between metals and chelating agents affects glutamate binding on brain synaptic membranes, Neurochem. Res. 28 (2003) 1859–1865, https://doi.org/10.1023/A:1026175825871.

[24] S.J.S. Flora, V. Pachauri, Chelation in metal intoxication, Int. J. Environ. Res. Publ. Health 7 (2010) 2745–2788, https://doi.org/10.3390/ijerph7072745.

[25] M.R. Awual, M.M. Hasand, J. Iqbalb, A. Islame, M.A. Islamf, A.M. Asiric, M. M. Rahman, Naked-eye lead(II) capturing from contaminated water using innovative large-pore facial composite materials, Microchem. J. 154 (2020) 104585, https://doi.org/10.1016/j.microc.2019.104585.

[26] M.R. Awual, M.M. Hasan, Novel conjugate adsorbent for visual detection and removal of toxic lead(II) ions from water, Microporous Mesoporous Mater. 196 (2014) 261–269, https://doi.org/10.1016/j.micromeso.2014.05.021.

[27] M.R. Awual, Mesoporous composite material for efficient lead(II) detection and removal from aqueous media, J. Environ. Chem. Eng. 7 (2019) 103124, https://doi.org/10.1016/j.jece.2019.103124.

[28] B. Yang, Y.H. Wei, Q.L. Liu, Y. Luo, S.Y. Qiu, Z.M. Shi, Polyvinylpyrrolidone functionalized magnetic graphene-based composites for highly efficient removal of lead from wastewater, Colloids Surf., A 582 (2019) 123927, https://doi.org/10.1016/j.colsurfa.2019.123927.

[29] M.R. Awual, M.M. Hasan, A ligand based innovative composite material for selective lead(II) capturing from wastewater, J. Mol. Liq. 294 (2019) 111679, https://doi.org/10.1016/j.molliq.2019.111679.

[30] P. Pan, J.-X. Fan, X.-N. Wang, J.-W. Wang, D.-W. Zheng, H. Cheng, X.-Z. Zhang, Bio-orthogonal bacterial reactor for remission of heavy metal poisoning and ROS elimination, Adv. Sci. (2019), https://doi.org/10.1002/advs.201902500, 1902500.

[31] X.Y. Guo, W.J. Wang, Y. Yang, Q.H. Tian, Y. Xiang, Y. Sun, Z.M. Bai, Magnetic nano capture agent with enhanced anion internal layer diffusion performance for removal of arsenic from human blood, Appl. Surf. Sci. 470 (2019) 296–305, https://doi.org/10.1016/j.apsusc.2018.11.135.

[32] H.Y. Lee, D.R. Bae, J.C. Park, H. Song, W.S. Han, J.H. Jung, A selective fluoroionophore based on BODIPY-functionalized magnetic silica nanoparticles: removal of Pb^{2+} from human blood, Angew. Chem. Int. Ed. 48 (2009) 1239–1243, https://doi.org/10.1002/anie.200804714.

[33] M.M. Wan, T.T. Xu, B. Chi, M. Wang, Y.Y. Huang, Q. Wang, T. Li, W.Q. Yan, H. Chen, P. Xu, C. Mao, B. Zhao, J. Shen, H. Xu, D.Q. Shi, A safe and efficient strategy for the rapid elimination of blood lead in vivo based on a capture-fix-separate mechanism, Angew. Chem. Int. Ed. 58 (2019) 10582–10586, https://doi.org/10.1002/ange.201904044.

[34] J.F. Ou, K. Liu, J.M. Jiang, D.A. Wilson, L. Liu, F. Wang, S.H. Wang, Y.F. Tu, F. Peng, Micro-/nanomotors toward biomedical applications: the recent progress in biocompatibility, Small 16 (2020) 1906184, https://doi.org/10.1002/smll.201906184.

[35] M.M. Wan, H. Chen, Q. Wang, Q. Niu, P. Xu, Y.Q. Yu, T.Y. Zhu, C. Mao, J. Shen, Bio-inspired nitric-oxide-driven nanomotor, Nat. Commun. 10 (2019) 966, https://doi.org/10.1038/s41467-019-08670-8.

[36] P.L. Venugopalan, B.E.-F.D. Avila, M. Pal, A. Ghosh, J. Wang, Fantastic voyage of nanomotors into the cell, ACS Nano 14 (2020) 9423–9439, https://doi.org/10.1021/acsnano.0c05217.

[37] T. Hou, S.S. Yu, M.F. Zhou, M. Wu, J. Liu, X.L. Zheng, J.X. Li, J. Wang, X.L. Wang, Effective removal of inorganic and organic heavy metal pollutants with poly(amino acid)-based micromotors, Nanoscale 12 (2020) 5227, https://doi.org/10.1039/c9nr09813e.

[38] T. Maric, C.C. Mayorga-Martinez, B. Khezri, M.Z.M. Nasir, X. Chia, M. Pumera, Nanorobots constructed from nanoclay: using nature to create self-propelled autonomous nanomachines, Adv. Funct. Mater. 28 (2018) 1802762, https://doi.org/10.1002/adfm.201802762.

[39] X. Wang, C. Ho, Y. Tsatskis, J. Law, Z. Zhang, M. Zhu, C. Dai, F. Wang, M. Tan, S. Hopyan, H. McNeill, Y. Sun, Intracellular manipulation and measurement with multipole magnetic tweezers, Sci. Robot. 4 (2019), eaav6180, https://doi.org/10.1126/scirobotics.aav6180.

[40] A.H.B.D. Vries, B.E. Krenn, R.V. Driel, J.S. Kanger, Micro magnetic tweezers for nanomanipulation inside live cells, Biophys. J. 88 (3) (2005) 2137–2144.

[41] M. Pal, N. Somalwar, A. Singh, R. Bhat, S.M. Eswarappa, D.K. Saini, A. Ghosh, Maneuverability of magnetic nanomotors inside living cells, Adv. Mater. 30 (2018) 1800429, https://doi.org/10.1002/adma.201800429.

[42] H. Chen, S.B. Shao, Y.Q. Yu, Y.Y. Huang, X.T. Zhu, S.Y. Zhang, J. Fan, G.Y. Yin, B. Chi, M.M. Wan, C. Mao, A dual-responsive biosensor for blood lead detection, Anal. Chim. Acta 1093 (2020) 131–141, https://doi.org/10.1016/j.aca.2019.09.062.

[43] M.K. Jaiswal, S. Mehta, R. Banerjee, D. Bahadur, A comparative study on thermoresponsive magnetic nanohydrogels: role of surface-engineered magnetic nanoparticles, Colloid Polym. Sci. 290 (2012) 607–617, https://doi.org/10.1007/s00396-011-2572-z.

[44] J. Sedlak, R.H. Lindsay, Estimation of total, protein-bound, and nonprotein sulfhydryl groups in tissue with Ellman's reagent, Anal. Biochem. 25 (1968) 192–205, https://doi.org/10.1016/0003-2697(68)90092-4.

[45] M.R. Awual, Innovative composite material for efficient and highly selective Pb(II) ion capturing from wastewater, J. Mol. Liq. 284 (2019) 502–510, https://doi.org/10.1016/j.molliq.2019.03.157.

[46] M.R. Awual, Novel conjugated hybrid material for efficient lead(II) capturing from contaminated wastewater, Mater. Sci. Eng. C 101 (2019) 686–695, https://doi.org/10.1016/j.msec.2019.04.015.

[47] Y.N. Zhang, Q. Jiang, S.B. Xie, X.W. Wu, J. Zhou, H. Sun, Lead induced ototoxicity and neurotoxicity in adult Guinea pig, BioMed Res. Int. 2019 (2019) 3626032, https://doi.org/10.1155/2019/3626032.

[48] H.C. Gonick, A.H. Cohen, Q. Ren, L.F. Saldanha, F. Khalil-Manesh, J. Anzalone, Y. Y. Sun, Effect of 2, 3-dimercaptosuccinic acid on nephrosclerosis in the Dahi rat. I. Role of reactive oxygen species, Kidney Int. 50 (1996) 1572–1581, https://doi.org/10.1038/ki.1996.473.

[49] M. Wang, W.Q. Yan, M.L. Chu, T. Li, Z.Y. Liu, Y.Q. Yu, Y.Y. Huang, T.Y. Zhu, M. M. Wan, C. Mao, D.Q. Shi, Erythrocyte membrane-wrapped magnetic nanotherapeutic agents for reduction and removal of blood Cr(VI), ACS Appl. Mater. Interfaces 12 (2020) 28014–28023, https://doi.org/10.1021/acsami.0c06437.

[50] M.M. Wan, Q. Wang, X.Y. Li, B. Xu, D. Fang, T. Li, Y.Q. Yu, L.Y. Fang, Y. Wang, M. Wang, F.H. Wang, C. Mao, J. Shen, J. Wei, Systematic research and evaluation models of nanomotors for cancer combined therapy, Angew. Chem. Int. Ed. 59 (2020) 2–10, https://doi.org/10.1002/anie.202002452.

[51] H. Li, Z.F. Chi, J.Z. Li, Covalent bonding synthesis of magnetic graphene oxide nanocomposites for Cr(III) removal, Desalin. Water Treat. 52 (2014) 10–12, https://doi.org/10.1080/19443994.2013.806224.

[52] P.G. Balkanloo, M. Mahmoudian, M.T. Hosseinzadeh, A comparative study between MMT-Fe_3O_4/PES, MMT-HBE/PES, and MMT-acid activated/PES mixed matrix membranes, Chem. Eng. J. 396 (2020) 125188, https://doi.org/10.1016/j.cej.2020.125188.

[53] S. Fatahian, D. Shahbazi-Gahrouei, M. Pouladian, M.H. Yousefi, G.R. Amiri, A. Noori, Biodistribution and toxicity assessment of radiolabeled and DMSA coated ferrite nanoparticles in mice, J. Radioanal. Nucl. Chem. 293 (2012) 915–921, https://doi.org/10.1007/s10967-012-1822-y.

[54] W.H. Chen, P.W. Yi, Y. Zhang, L.M. Zhang, Z.W. Deng, Z.J. Zhang, Composites of aminodextran-coated Fe_3O_4 nanoparticles and graphene oxide for cellular magnetic resonance imaging, ACS Appl. Mater. Interfaces 3 (2011) 4085–4091, https://doi.org/10.1021/am2009647.

[55] M. Qi, K. Zhang, S.Q. Li, J.R. Wu, C.O. Pham-Huy, X.T. Diao, D.L. Xiao, H. He, Superparamagnetic Fe_3O_4 nanoparticles: synthesis by a solvothermal process and functionalization for a magnetic targeted curcumin delivery system, New J. Chem. 40 (2016) 4480, https://doi.org/10.1039/c5nj02441b.

[56] X.-M. Wang, P.-F. Guo, Z.-J. Hu, M.-L. Chen, J.-H. Wang, DMSA-functionalized mesoporous alumina with a high capacity for selective isolation of immunoglobulin G, ACS Appl. Mater. Interfaces 11 (2019) 36286–36295, https://doi.org/10.1021/acsami.9b13718.

[57] X.Y. Guo, F.F. Mao, W.J. Wang, Y. Yang, Z.M. Bai, Sulfhydryl-modified Fe_3O_4@SiO_2 core/shell nanocomposite: synthesis and toxicity assessment in vitro, ACS Appl. Mater. Interfaces 7 (2015) 14983–14991, https://doi.org/10.1021/acsami.5b03873.

[58] W.J. Dong, Y.S. Li, D.C. Niu, Z. Ma, J.L. Gu, Y. Chen, W.R. Zhao, X.H. Liu, C.S. Liu, J.L. Shi, Facile synthesis of monodisperse superparamagnetic Fe_3O_4 core@hybrid@Au shell nanocomposite for bimodal imaging and photothermal therapy, Adv. Mater. 23 (2011) 5392–5397, https://doi.org/10.1002/adma.201103521.

[59] R. Devi, M. Bhatia, Thiol functionalization of flaxseed mucilage: preparation, characterization and evaluation as mucoadhesive polymer, Int. J. Biol. Macromol. 126 (2019) 101–106, https://doi.org/10.1016/j.ijbiomac.2018.12.116.

[60] C.-X. Du, T.-B. Zhang, S.-L. Dong, L. Han, X.-J. Liang, L.-H. Li, Y. Wei, A magnetic gene delivery nanosystem based on cationic liposomes, J. Mater. Sci. 51 (2016) 8461–8470, https://doi.org/10.1007/s10853-016-0106-2.

[61] S. Venkateswarlu, B.N. Kumar, B. Prathima, Y. SubbaRao, N.V.V. Jyothi, A novel green synthesis of Fe_3O_4 magnetic nanorods using Punica Granatum rind extract and its application for removal of Pb(II) from aqueous environment, Arabian J. Chem. 12 (2019) 588–596, https://doi.org/10.1016/j.arabjc.2014.09.006.

[62] C.Y. Yong, X.Q. Chen, Q. Xiang, Q. Li, X.D. Xing, Recyclable magnetite-silver heterodimer nanocomposites with durable antibacterial performance, Bioact. Mater. 3 (2018) 80–86, https://doi.org/10.1016/j.bioactmat.2017.05.008.

[63] Y.T. Yang, K.D. Jiang, J. Guo, J. Li, X.L. Peng, B. Hong, X.Q. Wang, H.L. Ge, Facile fabrication of Au/Fe_3O_4 nanocomposites as excellent nanocatalyst for ultrafast recyclable reduction of 4-nitropheol, Chem. Eng. J. 381 (2020) 122596.

[64] Q.L. Li, H.T. Chen, X.Y. Feng, C.C. Yu, F. Feng, Y.H. Chai, P. Lu, T. Song, X. Y. Wang, L. Yao, Nanoparticle-regulated semiartificial magnetotactic bacteria with tunable magnetic moment and magnetic sensitivity, Small 15 (2019) 1900427, https://doi.org/10.1002/smll.201900427.

[65] F. Gertz, A. Khitun, Biological cell manipulation by magnetic nanoparticles, AIP Adv. 6 (2016), 025308, https://doi.org/10.1063/1.4942090.

[66] Y.M. Qi, Y.J. Geng, B.H. Ma, Y. He, C.X. Cui, In vitro hemolytic properties'assessment of $K_2Ti_6O_{13}$ nanowires, J. Nanoeng. Nanosyst. 229 (2015) 201–205, https://doi.org/10.1177/1740349914529755.

[67] K.C. Zhang, J. Lia, Y.N. Wang, Y.Z. Mu, X.J. Sun, C. Su, Y. Dong, J.H. Pang, L. Huang, X.G. Chena, C. Feng, Hydroxybutyl chitosan/diatom-biosilica composite sponge for hemorrhage control, Carbohydr. Polym. 236 (2020) 116051, https://doi.org/10.1016/j.carbpol.2020.116051.

[68] M.M. Wan, Q. Wang, R.L. Wang, R. Wu, T. Li, D. Fang, Y.Y. Huang, Y.Q. Yu, L. Y. Fang, X.W. Wang, Y.H. Zhang, Z.Y. Miao, B. Zhao, F.H. Wang, C. Mao, Q. Jiang, X.Q. Xu, D.Q. Shi, Platelet-derived porous nanomotor for thrombus therapy, Sci. Adv. 6 (2020), https://doi.org/10.1126/sciadv.aaz9014 eaaz9014.

[69] E.R. Burns, S. Pollack, P. Falciparum infected erythrocytes are capable of endocytosis, In Vitro Cell. Dev. Biol. 24 (1988) 481–486, https://doi.org/10.1007/BF02628503.

[70] B.M. Rothen-Rutishauser, S. Schuerch, B. Haenni, N. Kapp, P. Gehr, Interaction of fine particles and nanoparticles with red blood cells visualized with advanced microscopic techniques, Environ. Sci. Technol. 40 (2006) 4353–4359, https://doi.org/10.1021/es0522635.

[71] P.U. Atukorale, Y.-S. Yang, A. Bekdemir, R.P. Carney, P.J. Silva, N. Watson, F. Stellaccic, D.J. Irvine, Influence of the glycocalyx and plasma membrane composition on amphiphilic gold nanoparticle association with erythrocytes, Nanoscale 7 (2015) 11420–11432, https://doi.org/10.1039/c5nr01355k.

[72] M.R. Awual, Assessing of lead(III) capturing from contaminated wastewater using ligand doped conjugate adsorbent, Chem. Eng. J. 289 (2016) 65–73, https://doi.org/10.1016/j.cej.2015.12.078.

[73] M.R. Awual, A novel facial composite adsorbent for enhanced copper(II) detection and removal from wastewater, Chem. Eng. J. 266 (2015) 368–375, https://doi.org/10.1016/j.cej.2014.12.094.

[74] H.X. Duan, X. Hu, Z.R. Sun, Magnetic zeolite imidazole framework material-8 as an effective and recyclable adsorbent for removal of ceftazidime from aqueous solution, J. Hazard Mater. 384 (2020) 121406, https://doi.org/10.1016/j.jhazmat.2019.121406.

[75] A. Shahata, H.M.A. Hassana, H.M.E. Azzazyc, E.A. El-Sharkawya, H.M. Abdoud, M. R. Awual, Novel hierarchical composite adsorbent for selective lead(II) ions capturing from wastewater samples, Chem. Eng. J. 332 (2018) 377–386, https://doi.org/10.1016/j.cej.2017.09.040.

[76] A. Shahat, M.R. Awual, M.A. Khaleque, M.Z. Alam, M. Naushad, A.M. S. Chowdhury, Large-pore diameter nano-adsorbent and its application for rapid lead(II) detection and Removal from aqueous media, Chem. Eng. J. 273 (2015) 286–295, https://doi.org/10.1016/j.cej.2015.03.073.

[77] F. Beduk, Superparamagnetic nanomaterial Fe_3O_4-TiO_2 for the removal of as (V) and As(III) from aqueous solutions, Environ. Technol. 37 (2016) 1790–1801, https://doi.org/10.1080/09593330.2015.1132777.

[78] M. Shafiee, R. Foroutan, K. Fouladi, M. Ahmadlouydarab, B. Ramavandi, S. Sahebi, Application of oak powder/Fe_3O_4 magnetic composite in toxic metals removal from aqueous solutions, Adv. Powder Technol. 30 (2019) 544–554, https://doi.org/10.1016/j.apt.2018.12.006.

[79] Y. Cao, X. Hu, C.Q. Zhu, S.X. Zhou, R. Li, H.L. Shi, S.Y. Miao, M. Vakili, W. Wang, D.L. Qi, Sulfhydryl functionalized covalent organic framework as an efficient adsorbent for selective Pb(II) removal, Colloids Surf., A 600 (2020) 125004, https://doi.org/10.1016/j.colsurfa.2020.125004.

[80] P.P. Zhao, X.G. Xu, X.X. Zhao, C.Y. Ai, K.Y. Xu, M.X. Li, C.M. Jiang, J.L. Shi, Capability of bacillus subtilis to remove Pb^{2+} via producing lipopeptides, Sci. Total Environ. 730 (2020) 138941, https://doi.org/10.1016/j.scitotenv.2020.138941.

[81] H. Lai, J.S. Deng, S. Wen, Q.J. Liu, Elucidation of lead ions adsorption mechanism on marmatite surface by PCA-assisted ToF-SIMS, XPS and zeta potential, Miner. Eng. 144 (2019) 106035, https://doi.org/10.1016/j.mineng.2019.106035.

[82] Q. Jiang, W.L. Xie, S.Y. Han, Y.F. Wang, Y. Zhang, Enhanced adsorption of Pb(II) onto modified hydrochar by polyethyleneimine or H_3PO_4: an analysis of surface

property and interface mechanism, Colloids Surf., A 583 (2019) 123962, https://doi.org/10.1016/j.colsurfa.2019.123962.
[83] O.F. Odio, L. Lartundo-Rojas, E.G. Palacios, R. Martínez, E. Reguera, Synthesis of a novel poly-thiolated magnetic nano-platform for heavy metal adsorption. Role of thiol and carboxyl functions, Appl. Surf. Sci. 386 (2016) 160–177, https://doi.org/10.1016/j.apsusc.2016.05.176.
[84] D.G. Castner, X-ray photoelectron spectroscopy sulfur 2p study of organic thiol and disulfide binding interactions with gold surfaces, Langmuir 12 (1996) 5083–5086, https://doi.org/10.1021/la960465w.